Static Self-Energy and Effective Mass of the Homogeneous Electron Gas from Quantum Monte Carlo Calculations

Markus Holzmann,[1] Francesco Calcavecchia,[1] David M. Ceperley[ORCID],[2] and Valerio Olevano[3]

[1]*Univ. Grenoble Alpes, CNRS, LPMMC, 38000 Grenoble, France*
[2]*University of Illinois Urbana-Champaign, Urbana, Illinois 61801, USA*
[3]*CNRS, Institut Néel, 38042 Grenoble, France*

We discuss the methodology of quantum Monte Carlo calculations of the effective mass based on the static self-energy $\Sigma(k,0)$. We then use variational Monte Carlo calculations of $\Sigma(k,0)$ of the homogeneous electron gas at various densities to obtain results very close to perturbative $G_0 W_0$ calculations for values of the density parameter $1 \leq r_s \leq 10$. The obtained values for the effective mass are close to diagrammatic Monte Carlo results and disagree with previous quantum Monte Carlo calculations based on a heuristic mapping of excitation energies to those of an ideal gas.

Landau's Fermi liquid theory [1] has provided a paradigmatic frame for the phenomenological description of equilibrium and transport properties of degenerate fermions in terms of a very few characteristic parameters. Silin [2] has provided the path to generalize for long-range forces, in order to extend it to normal metals in condensed matter [3,4]. Although the formal structure of the underlying microscopic theory has been known for a long time [5–7], most explicit calculations of the Fermi liquid parameters rely on approximative, perturbative schemes [8,9]. As diagrammatic perturbation theory is not expected to converge for typical electronic densities, basic Fermi liquid parameters of the 3D homogeneous electron gas (jellium), such as the effective mass m^* and the renormalization factor Z, are sensitive to the underlying approximation [10,11] (see also Fig. 4 of Ref. [12]).

Recently, variational diagrammatic Monte Carlo calculations (VDiagMC) [13,14] for 3D jellium have been performed to include and control higher order terms of the perturbation series. Those calculations found an overall reasonable agreement for Z with previous quantum Monte Carlo (QMC) calculations [15]. However, VDiagMC results on m^* have been strongly questioned by QMC calculations of Ref. [12] yielding substantially different values.

In this Letter, we revisit the methodology of zero temperature QMC calculations of the effective mass, in order to resolve the discrepancy between QMC and perturbative-VDiagMC results, show how such calculations can be done, and provide new results for 3D jellium. In principle, the effective mass can also be calculated from the temperature dependence of thermodynamic quantities [16,17], e.g., from finite-temperature path-integral results [18–20]; finite temperature methods will not be discussed here. In contrast to systems with short range

interaction [21], size corrections are expected to play an important role for charged systems [22] as explained in detail below.

Landau energy functional.—Landau [1] phenomenologically characterized the low energy excitation of a Fermi liquid by assuming a one-to-one correspondence of states of the ideal Fermi gas and those of the interacting system, such that elementary excitations of the interacting systems are still described in terms of ideal gas occupation numbers before adiabatically switching on the interaction. Changes of the total energy δE can then be considered as a functional of changes in the quasiparticle occupation number $\delta n_{k\sigma}$ of the momentum k and spin quantum number σ

$$\delta E = \sum_{k\sigma}(\varepsilon_k + \mu)\delta n_{k\sigma} + \frac{1}{2V}\sum_{k\sigma,k'\sigma'} f(k\sigma,k'\sigma')\delta n_{k\sigma}\delta n_{k'\sigma'}. \quad (1)$$

Here, μ is the chemical potential, $\varepsilon_k = (k - k_F)k_F/m^*$ is the quasiparticle energy which determines the effective mass for momenta in the vicinity of the Fermi momentum k_F, and $f(k\sigma,k'\sigma')$ is the quasiparticle interaction, independent of volume V to leading order. Here, and in the following, we assume a homogeneous system with isotropic Fermi surface and set $\hbar = 1$.

The success of Landau's Fermi liquid theory started with its application to strongly interacting quantum liquids [23]. Postulating an entropy functional in terms of quasiparticle occupations, nontrivial predictions could be made using only a few parameters, notably the effective mass entering the quasiparticle energy ε_k.

Fermi liquid behavior results from the assumption of certain analytical properties of fundamental correlation functions [7], notably the existence of a Fermi surface [6] defined by the sharp discontinuity Z of the momentum

distribution at zero temperature, and the effective mass m^* obtained from the dispersion of the quasiparticle peak of the spectral function.

Both quantities Z and m^* can thus be operationally defined from the single particle Green's function, conveniently expressed in Fourier space,

$$G(k, z) = G^+(k, z) + G^-(k, z), \qquad (2)$$

$$G^\pm(k, z) = \sum_n \frac{|\langle E_n^{N\pm1}|(a_k^\dagger + a_k)|E_0^N\rangle|^2}{z - (\pm(E_n^{N\pm1} - E_0^N) - \mu)}, \qquad (3)$$

where $|E_n^N\rangle$ denotes the nth eigenstate with energy E_n^N of the N-particle system and a_k annihilates an electron of wavevector k. The self-energy Σ defined as

$$G^{-1}(k, z) = z + \mu - k^2/2m - \Sigma(k, z) \qquad (4)$$

captures all effects of interactions where m is the bare mass. The Fermi surface is then determined from $G^{-1}(k_F, 0) = 0$, or $\mu = k_F^2/2m + \Sigma(k_F, 0)$. The analytic structure of G close to the singularity determines Fermi liquid behavior. Under quite general assumptions the self-energy of the infinite system allows an expansion [7,24]

$$\Sigma(k, z) - \Sigma(k_F, 0) = (k - k_F)\partial_k\Sigma(k_F, 0) + z\partial_z\Sigma(k_F, 0) \qquad (5)$$

up to corrections of order k^2 and $z^2 \log z$. The singularity dominating the Green's function close to the Fermi surface is then

$$G(k, z) \sim \frac{Z}{z - (k - k_F)k_F/m^*}, \qquad (6)$$

with

$$Z^{-1} = 1 - \partial_z\Sigma(k_F, 0), \qquad (7)$$

$$\frac{m}{m^*} = Z\left(1 + \frac{m}{k_F}\partial_k\Sigma(k_F, 0)\right), \qquad (8)$$

giving rise to a well defined quasiparticle behavior of strength Z and energy $(k - k_F)k_F/m^*$. Since $G(k, 0)$ changes sign at $k = k_F$, the singularity of the Green's function close to the Fermi surface is entirely contained in either $G^+(k, z)$ or $G^-(k, z)$. The real-time spectral function is obtained by approaching the real axis using $z = i\omega + \eta_k$ where $\eta_k = +0$ (-0) for $k > k_F$ $(k < k_F)$.

Landau's energy functional may then be identified with the quasiparticle energies of the single particle propagator [4,6], providing a microscopic expression for the quasiparticle occupation number [4,7]. As knowledge of the quasiparticle energy is explicitly required and its definition involves off-diagonal matrix elements in the energy eigenstate representation, this definition is purely formal and has not been of much practical use. However, it provides a strong indication that Landau's quasiparticle occupation number may not be expressible as a simple static observable whose value can be determined from a single energy eigenstate. Only in the limit $k \to k_F$ does the quasiparticle energy approximate an exact energy eigenstate up to corrections of the order of the inverse lifetime [7], provided the thermodynamic limit is taken first.

Both Z and m^* can be obtained from static observables at zero temperature. The value of the renormalization constant Z can be read off from the jump in the momentum distribution [15], whereas $\Sigma(k, 0)$ can be obtained from the static response to an external perturbation $\xi(a_k + a_k^\dagger)$ as we will show below. Together they can be used to calculate m^* very near to the Fermi surface.

Landau's Fermi liquid theory successfully describes thermal equilibrium or hydrodynamic transport observables [23], i.e., bulk properties. The form of Landau's energy functional, Eq. (1), assures that its energy changes with respect to variation of the quasiparticle occupations are to first order additive, with corrections from a small, $\sim1/V$, pairwise interaction. Although these energy variations can be mapped to variations of the unperturbed ideal gas propagator within adiabatic perturbation theory [7], they cannot, in general, be mapped to the exact excited energy eigenstates of the interacting system.

The microscopic theory maps them to the single particle quasiparticle spectrum, characterized by the emerging pole in the exact interacting propagator, Eq. (6), when approaching the real axis, $z = i\omega + \eta_k$ with $\eta_k \to \pm0$. However, for any finite system, the exact Green's function, Eq. (2) is a highly irregular function on the real axis; a smooth function can only be expected at a finite distance from the real axis, $|\eta_k|\gtrsim k_F 2\pi/(mL)$. Instead, the effective mass formula, Eq. (8), involves only static quantities with $z = 0$ and is well defined on the real axis, even before the thermodynamic limit is performed. Their calculations may still suffer from important finite-size effects [22], but numerical extrapolations will eventually converge to the infinite system size values.

Considering the generalized Hamiltonian $\tilde{H} = \sum_N(H_N - \mu N)$, an external perturbation $\xi(a_k + a_k^\dagger)$ couples the ground state of the N particle systems to excitations containing $N \pm 1$ particles. From time-independent perturbation theory, restricting to states $|E^+\rangle$ within the subspace of N and $N + 1$ particles, the perturbed ground state up to linear order in ξ can be written as

$$|E_k^+(\xi)\rangle = |E_0^N\rangle - \xi\sum_n \frac{|E_n^{N+1}\rangle\langle E_n^{N+1}|a_k^\dagger|E_0^N\rangle}{E_n^{N+1} - E_0^N - \mu} \qquad (9)$$

yielding the energy to second order in ξ:

$$E_k^+(\xi) = E_0^N + \mu - \xi^2 \sum_n \frac{|\langle E_n^{N+1}|a_k^\dagger|E_0^N\rangle|^2}{E_n^{N+1} - E_0^N - \mu}. \quad (10)$$

Similarly, E_k^- is the ground state of the perturbed Hamiltonian restricted to the N and $N-1$ subspaces. The Green's functions are determined by comparing with the Lehmann representation, Eq. (2),

$$G^\pm(k,0) = \lim_{\xi\to 0}[\pm(E_k^\pm(\xi) - E_0^N) - \mu]/\xi^2. \quad (11)$$

Upper bounds to the ground state energies $E_k^\pm$ can be obtained with a variational ansatz for $|E_k^\pm\rangle$ and minimizing the expectation value of the perturbed Hamiltonian with respect to variational parameters. Although technically a little bit more involved, calculations of the static Green's function are thereby reduced to a static response function, analogous to calculations of the density response [25] previously employed using ground state Monte Carlo methods.

Quantum Monte Carlo calculations.—Let us now turn to the calculation of the static single-particle Green's function via quantum Monte Carlo methods, focusing on $G^+(k,0)$. For that, we minimize the energy $E_T^+(\xi)$ of the generalized Hamiltonian $\tilde{H}$ using a trial wave function $|\Psi_T(\xi)\rangle$ in the Fock space of N and $N+1$ particle wave functions providing an upper bound for $E_k^+(\xi)$.

Assuming that ξ is sufficiently small, the trial wave function can be expanded as

$$|\Psi_T(\xi)\rangle = |\Psi_0^N\rangle + \xi \sum_{i=1}^M \alpha_i|\Psi_i^{N+1}\rangle, \quad (12)$$

with M the number of states in the basis. It couples the ground state wave function $|\Psi_0^N\rangle$ of the N particle system (or our best variational ground state wave function) with different wave functions $|\Psi_i^{N+1}\rangle$ of the $N+1$ particle states of total momentum corresponding to k. The variational parameters are the set $\{\alpha_i\}$. Here, we choose $M=2$, with $|\Psi_1^{N+1}\rangle$ as a candidate for a pure excited state wave function, minimizing separately the excited state energy E_k^{N+1} in the $N+1$ section of momentum k, and $|\Psi_2^{N+1}\rangle \sim a_k^\dagger|\Psi_0^N\rangle$; this should maximize the overlap matrix elements of the perturbation with the ground state, e.g., the numerator of the right-hand side of Eqs. (9) and (10).

Minimizing with respect to α_1, α_2 in the limit of $\xi \to 0$, we obtain a variational approximation for the Green's function in the particle excitation sector

$$G_\mu^+(k,0) = -\frac{\zeta_1^2\varepsilon_{22} - 2\zeta_1\zeta_2\varepsilon_{12} + \zeta_2^2\varepsilon_{11}}{\varepsilon_{11}\varepsilon_{22} - \varepsilon_{12}^2}, \quad (13)$$

with $\quad \varepsilon_{ij} = \langle\Psi_i^{N+1}|H_{N+1} - E_0^N - \mu|\Psi_j^{N+1}\rangle, \quad (14)$

$$\zeta_i = \langle\Psi_i^{N+1}|a_k^\dagger|\Psi_0^N\rangle, \quad (15)$$

where we have assumed normalized wave functions, e.g., $\langle\Psi_i^{N\pm 1}|\Psi_i^{N\pm 1}\rangle = 1$, with overall phases such that all matrix elements are real.

An analogous calculation in the hole sector yields $G_\mu^-(k,0)$ from a variational calculation based on superposition of the lowest energy state for a hole excitation and $a_k|\Psi_0^N\rangle$. Thus, the static Green's function $G_\mu(k,0) = G_\mu^+(k,0) + G_\mu^-(k,0)$ is determined.

Let us stress that our determination of the static Green's function is strictly variational providing upper (lower) bounds for the perturbed energies by electron (hole) addition and does not rely on perturbation theory. The exact Green's function is approached for a sufficiently flexible wave function $\Psi^{N\pm 1}$, as can be seen from a spectral (Lehmann) representation.

So far, the chemical potential μ, entering as a parameter in $G_\mu^\pm$, has not been specified yet. Since single particle excitation is gapless in the Fermi liquid, the chemical potential can be fixed by the implicit equation $\lim_{k\to k_F} G_\mu^{-1}(k,0) = 0$.

Finite size effects.—Our quantum Monte Carlo calculations are done for a finite number of electrons N confined in a periodic cube of side L and volume $V = L^3$. Calculations must be extrapolated to the thermodynamic limit. Shell effects in the single particle energy spectrum and the Coulombic interaction represent the main source of finite size effects [26].

Shell effects can be addressed by twisted boundary conditions [27] corresponding to a shifted grid calculation in momentum space. Using grand-canonical twist averaging (GC-TABC) [28] we obtain a sharp Fermi surface. We spherically average $G_\mu^\pm(k,0)$ for any k using 32 equally weighted points that exactly integrates all polynomials on the sphere up to the eighth order [29,30].

Although GC-TABC allows us to obtain $G_\mu^\pm(k,0)$ for arbitrary k, size effects due to intrinsic two-body effects remain. In charged systems, these are dominated by the long-range Coulomb interaction [31,32]. In particular, z_k and n_k are expected to suffer from important size effects [15] of order $1/L$. Instead of addressing them directly which necessitates a thorough investigation as a function of L and k, we will determine the exact leading order form of the corrections from a diagrammatic analysis based on Fermi liquid theory [7]. Following Ref. [22], within the random phase approximation (RPA) approximation, $\delta\Sigma(k,0) = \Sigma_\infty(k,0) - \Sigma_N(k,0)$ is given by

$$\delta\Sigma(k,0) \simeq -\int_{-\pi/L}^{\pi/L} \frac{d^3q}{(2\pi)^3} \int_{-\infty}^\infty \frac{d\nu}{(2\pi)} \frac{v_q}{\epsilon(q,i\nu)} \frac{1}{i\nu + \mu - \varepsilon_{k+q}^0}, \quad (16)$$

where $v_q = 4\pi e^2/q^2$ is the Coulomb interaction, $\varepsilon_k^0 = \hbar^2 k^2/2m$, and the integral is restricted to a cube with $|q_\alpha| < \pi/L$ for any spatial component ($\alpha = x$, y, z).
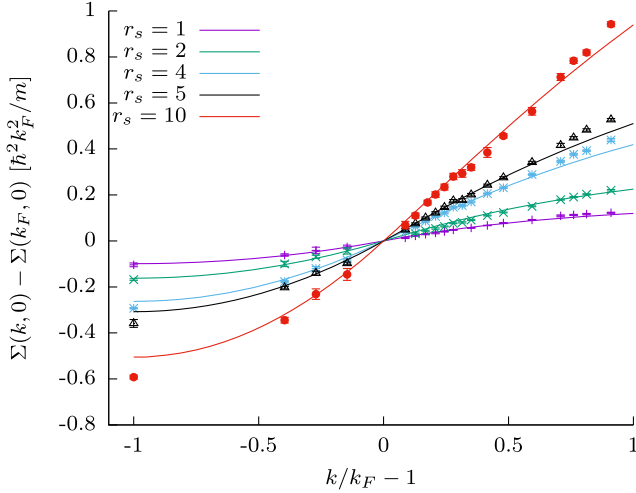
FIG. 1. Static self-energy for various densities (r_s) using backflow (BF) trial wave functions and GC-TABC simulations for $N = 38$ electrons. They include size corrections. The color lines are from G_0W_0 calculations.

Because of this restriction, we can use the expression $\epsilon(q, \omega) \simeq 1 - \omega_p^2/\omega$ for the dielectric function, where ω_p is the plasma frequency. Since the dominant contribution to the integral stems from the finite values of $\omega = i\nu$, substituting this limiting form for the dielectric function captures the exact behavior in the limit of small q. The resulting integration then gives

$$\delta\Sigma(k, 0) = C \frac{\epsilon_k^0 - \mu}{\omega_p + |\epsilon_k^0 - \mu|}, \tag{17}$$

with $C \simeq 1.22 e^2/L$. One can show that Eq. (17) is indeed exact not only within RPA, if $\epsilon_k^0 - \mu$ is replaced by the exact single particle energies $(k - k_F)k_F/m^*$. This occurs since irreducible vertex corrections approach $1/Z$ in the limit of vanishing momentum transfer at fixed frequency [7] and exactly cancel against the quasiparticle weight of the exact propagator replacing the noninteracting propagator in the RPA expression.

Results and discussion.—We have performed variational Monte Carlo (VMC) calculations of the self-energy for the 3D homogeneous electron gas, shown in Fig. 1, based on analytical Slater-Jastrow (SJ) and Slater-Jastrow backflow (BF) wave functions [33,34] as used in a previous study on the renormalization factor [15]. Its density n is parametrized by $r_s \equiv a/a_B$, where a_B is the Bohr radius and $a = (4\pi n/3)^{-1/3}$ is the mean electron distance. Details of the VMC procedure are given in Supplemental Material [35].

In Fig. 2 we illustrate the importance of size effects at $r_s = 10$, comparing canonical simulations with periodic boundary conditions (PBC) from system sizes, $N = 38$ to 114 using SJ wave functions. Although, the bare curves seem to indicate only small variations with size, the size
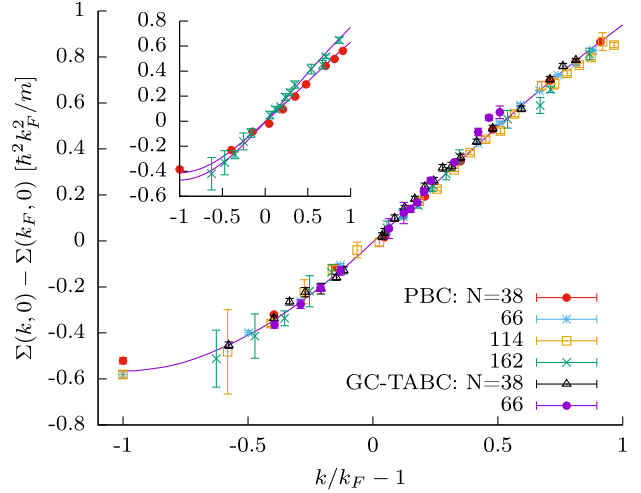
FIG. 2. Static self-energy for $r_s = 10$ using SJ-VMC trial wave functions for simulations with periodic boundary conditions (PBC) and GC-TABC for various sizes ranging from $N = 38$ to $N = 162$, size corrected according to Eq. (17), the line is a fit to the data, taking into account small difference to G_0W_0. The inset shows the uncorrected values for $N = 38$ and $N = 162$ (PBC), the lines are obtained subtracting the size corrections, Eq. (17), from the fit of the extrapolated data in the main figure.

corrected curves based on the analytical formula above show that the bare curves for such small systems are still very far from reaching the thermodynamic limit. Because of the slow decay $\sim L$ of the corrections, we have not attempted any numerical extrapolation of the curves. Extrapolation is more difficult for smaller values of r_s since variations are masked by the larger stochastic error.

In Fig. 1 we compare our size corrected results from BF-VMC calculations using grand-canonical twist averaging to perturbative G_0W_0 results of the infinite system. Even though $r_s = 10$ is thought to be far outside the range of validity of a perturbative approach our QMC results indicate only small modifications in the whole range $r_s \leq 10$; differences are hardly visible on the figures. Uncorrected data at finite N are similarly close to G_0W_0 curves when finite size effects are accounted by subtracting Eq. (17) (see also Supplemental Material [35]).

In contrast to Z, perturbative calculations of $\partial_k\Sigma(k_F, 0)$ seem to be much less sensitive to the underlying approximation scheme, e.g., self-consistency and vertex corrections [11,36]. We do not believe that the quantitative agreement of the static self-energy between QMC and G_0W_0 is a result of fortuitous error cancellations.

In order to deduce the effective mass, we have fitted our QMC results for $\Sigma(k, 0)$ around k_F to obtain $\partial_k\Sigma(k_F, 0)$. In Table I we summarize our results based on size corrected GC-TABC calculations for $N = 66$ SJ and $N = 54$ BF wave functions. We see that the decrease of Z competes with the increase of $\partial_k\Sigma(k_F, 0)$, resulting in values of m^*/m very close to one. However, since $mk_F^{-1}\partial_k\Sigma(k_F, 0)$ remains smaller than one even at $r_s = 10$, the lowering of Z with

TABLE I. Our QMC results with backflow (BF) and Slater-Jastrow (SJ) trial functions as compared to those of G_0W_0 (RPA) and variational diagrammatic Monte Carlo (VDiagMC) [14,37,38]. Upper and lower indices indicate systematic errors assuming different fitting functions and ranges to determine $\partial_k\Sigma(k_F, 0)$.

r_s	Method	Z	$mk_F^{-1}\partial_k\Sigma$	m^*/m
1	BF-VMC	0.86(1) [15]	$0.17_{0.15}^{0.18}(1)$	$1.00_{0.99}^{1.01}(1)$
	SJ-VMC	0.894(9) [15]	$0.17_{0.15}^{0.18}(1)$	$0.96_{0.95}^{0.97}(1)$
	G_0W_0 (RPA)	0.859 [39]	0.200	0.970 [10]
	VDiagMC [14]	0.8725(2)	0.200(1)	0.955(1)
2	BF-VMC	0.78(1)	$0.309_{0.280}^{0.361}(6)$	$0.98_{0.94}^{1.00}(1)$
	SJ-VMC	0.82(1)	$0.30_{0.28}^{0.31}(2)$	$0.94_{0.93}^{0.95}(2)$
	G_0W_0 (RPA)	0.768 [39]	0.313	0.992 [10]
	VDiagMC [14]	0.7984(2)	0.328(4)	0.943(3)
4	BF-VMC	0.65(1)	$0.538_{0.530}^{0.549}(7)$	$1.00_{0.99}^{1.01}(2)$
	SJ-VMC	0.69(1)	$0.55_{0.45}(2)$	$0.94_{1.00}(2)$
	G_0W_0 (RPA)	0.646 [39]	0.490	1.039 [10]
	VDiagMC [14]	0.6571(2)	0.528(5)	0.996(3)
5	BF-VMC	0.59(1)	$0.56^{0.65}(1)$	$1.09_{1.03}(3)$
	SJ-VMC	0.61(1)	$0.610_{0.596}^{0.624}(9)$	$1.02_{1.01}^{1.03}(2)$
	G_0W_0 (RPA)	0.602 [39]	0.569	1.059 [10]
10	BF-VMC	0.41(1)	$0.90_{0.88}^{0.98}(2)$	$1.28_{1.23}^{1.30}(3)$
	SJ-VMC	0.45(1)	$0.97_{0.91}^{1.03}(3)$	$1.13_{1.09}^{1.16}(3)$
	G_0W_0 (RPA)	0.45 [39]	0.98	1.13

increasing r_s eventually dominates the effective mass and m^* clearly increases for $r_s \gtrsim 4$.

Similarly to Z, the change from the SJ trial function to more accurate BF trial functions reduces $\partial_k\Sigma(k_F, 0)$ by a small amount, slightly larger than our statistical resolution. This provides a rough estimate of the bias due to the trial wave function. Since our approach is variational, we expect that our results provide upper bounds to $\partial_k\Sigma$. In addition, more correlated wave functions tend to lower the values of Z [15,40], so that our results for m^* are likely lower bounds. Future studies based on iterative backflow and machine learning wave functions [40–43] can be used to further improve the wave function. Preliminary results for the momentum distribution [40] do not indicate noticeable bias beyond BF.

Our results are in rather good agreement with perturbative G_0W_0 calculations [10,39] and more recent variational diagrammatic Monte Carlo calculations including higher order diagrams [14,37]. They are at variance with previous QMC calculations [12] of m^* which are based on a heuristic mapping of excitation energies to the ideal gas and not on the properties of the single particle Green's function. As we have reviewed above, the use of Landau's energy functional to determine Fermi liquid parameters from the excitation spectrum of finite systems is highly problematic. The comparison with those results is further detailed in Supplemental Material [35]. Our methodology can be applied to realistic strongly correlated systems as well as

to quantum chemistry based methods addressing ground and excited state wave functions of finite systems [44,45].

The quantitative agreement between two methodologically and numerically different methods, real space QMC and VDiagMC, is highly encouraging. Comparisons with high precision measurements, as already done in solid sodium [46] and lithium [47,48] for the renormalization factor Z can now be extended to the band width and effective mass.

[1] L. D. Landau, Zh. Eksp. Teor. Fiz. **30**, 1058 (1956) [Sov. Phys. JETP **3**, 920 (1957)].
[2] V. P. Silin, Zh. Eksp. Teor. Fiz. **33**, 495 (1957) [Sov. Phys. JETP **6**, 387 (1958)].
[3] P. Noziéres and J. P. Luttinger, Phys. Rev. **127**, 1423 (1962).
[4] J. M. Luttinger and P. Noziéres, Phys. Rev. **127**, 1431 (1962).
[5] L. D. Landau, Zh. Eksp. Teor. Fiz. **35**, 97 (1958) [Sov. Phys. JETP **8**, 70 (1959)].
[6] J. M. Luttinger, Phys. Rev. **119**, 1153 (1960).
[7] P. Nozières, *Theory of Interacting Fermi Systems* (W.A. Benjamin, Inc., New York, 1964).
[8] G. F. Giuliani and G. Vignale, *Quantum Theory of the Electron Liquid* (Cambridge University Press, Cambridge, England, 2005).
[9] R. M. Martin, L. Reining, and D. M. Ceperley, *Interacting Electrons* (Cambridge University Press, Cambridge, England, 2016).
[10] G. E. Simion and G. F. Giuliani, Phys. Rev. B **77**, 035131 (2008).
[11] A. L. Kutepov and G. Kotliar, Phys. Rev. B **96**, 035108 (2017).
[12] S. Azadi, N. D. Drummond, and W. M. C. Foulkes, Phys. Rev. Lett. **127**, 086401 (2021).
[13] K. Chen and K. Haule, Nat. Commun. **10**, 3725 (2019).
[14] K. Haule and K. Chen, Sci. Rep. **12**, 2294 (2022).
[15] M. Holzmann, B. Bernu, C. Pierleoni, J. McMinis, D. M. Ceperley, V. Olevano, and L. Delle Site, Phys. Rev. Lett. **107**, 110402 (2011).
[16] F. G. Eich, M. Holzmann, and G. Vignale, Phys. Rev. B **96**, 035132 (2017).
[17] H. Xie, L. Zhang, and L. Wang, SciPost Phys. **14**, 154 (2023).
[18] E. W. Brown, B. K. Clark, J. L. DuBois, and D. M. Ceperley, Phys. Rev. Lett. **110**, 146405 (2013).
[19] E. W. Brown, J. L. DuBois, M. Holzmann, and D. M. Ceperley, Phys. Rev. B **88**, 081102(R) (2013); **88**, 199901(E) (2013).

[20] T. Dornheim, S. Groth, and M. Bonitz, Phys. Rep. **744**, 1 (2018).

[21] E. Vitali, H. Shi, M. Qin, and S. Zhang, Phys. Rev. B **94**, 085140 (2016).

[22] M. Holzmann, B. Bernu, and D. M. Ceperley, J. Phys. Conf. Ser. **321**, 012020 (2011).

[23] G. Baym and C. J. Pethick, *Landau Fermi-Liquid Theory: Concepts and Applications* (Wiley, New York, 2008).

[24] A. B. Migdal, *Theory of Finite Fermi Systems and Application to Atomic Nuclei* (Wiley, New York, 1967).

[25] S. Moroni, D. M. Ceperley, and G. Senatore, Phys. Rev. Lett. **69**, 1837 (1992).

[26] M. Holzmann, R. C. Clay, M. A. Morales, N. M. Tubman, D. M. Ceperley, and C. Pierleoni, Phys. Rev. B **94**, 035126 (2016).

[27] C. Lin, F.-H. Zong, and D. M. Ceperley, Phys. Rev. E **64**, 016702 (2001).

[28] M. Holzmann, B. Bernu, V. Olevano, R. M. Martin, and D. M. Ceperley, Phys. Rev. B **79**, 041308(R) (2009).

[29] R. Womersley, Efficient Spherical Designs with Good Geometric Properties, https://web.maths.unsw.edu.au/~rsw/Sphere/EffSphDes/ss.html.

[30] R. S. Womersley, in *Contemporary Computational Mathematics—A Celebration of the 80th Birthday of Ian Sloan*, edited by J. Dick, F. Kuo, and H. Woźniakowski (Springer, Cham, 2018).

[31] S. Chiesa, D. M. Ceperley, R. M. Martin, and M. Holzmann, Phys. Rev. Lett. **97**, 076404 (2006).

[32] Y. Yang, V. Gorelov, C. Pierleoni, D. M. Ceperley, and M. Holzmann, Phys. Rev. B **101**, 085115 (2020).

[33] Y. Kwon, D. M. Ceperley, and R. M. Martin, Phys. Rev. B **48**, 12037 (1993).

[34] M. Holzmann, D. M. Ceperley, C. Pierleoni, and K. Esler, Phys. Rev. E **68**, 046707 (2003).

[35] See Supplemental Material at http://link.aps.org/supplemental/10.1103/PhysRevLett.131.186501 for more details on the VMC calculations.

[36] K. Van Houcke, I. S. Tupitsyn, A. S. Mishchenko, and N. V. Prokof'ev, Phys. Rev. B **95**, 195131 (2017).

[37] Results given in [14] are obtained at finite electronic temperature $T = T_F/25$ where T_F is the Fermi temperature and may be modified by zero temperature extrapolation.

[38] VDiagMC and G_0W_0 values for $\partial_k \Sigma_\infty$ are obtained using those given for Z and m^*/m, assuming that the respective error is statistically independent.

[39] L. Hedin, Phys. Rev. **139**, A796 (1965).

[40] M. Wilson, S. Moroni, M. Holzmann, N. Gao, F. Wudarski, T. Vegge, and A. Bhowmik, Phys. Rev. B **107**, 235139 (2023).

[41] M. Taddei, M. Ruggeri, S. Moroni, and M. Holzmann, Phys. Rev. B **91**, 115106 (2015).

[42] M. Holzmann and S. Moroni, Phys. Rev. Lett. **124**, 206404 (2020).

[43] G. Cassella, H. Sutterud, S. Azadi, N. D. Drummond, D. Pfau, J. S. Spencer, and W. M. C. Foulkes, Phys. Rev. Lett. **130**, 036401 (2023).

[44] J. J. Shepherd, G. H. Booth, and A. Alavi, J. Chem. Phys. **136**, 244101 (2012).

[45] J. J. Shepherd and A. Grüneis, Phys. Rev. Lett. **110**, 226401 (2013).

[46] S. Huotari, J. A. Soininen, T. Pylkkänen, K. Hämäläinen, A. Issolah, A. Titov, J. McMinis, J. Kim, K. Esler, D. M. Ceperley, M. Holzmann, and V. Olevano, Phys. Rev. Lett. **105**, 086403 (2010).

[47] N. Hiraoka, Y. Yang, T. Hagiya, A. Niozu, K. Matsuda, S. Huotari, M. Holzmann, and D. M. Ceperley, Phys. Rev. B **101**, 165124 (2020).

[48] Y. Yang, N. Hiraoka, K. Matsuda, M. Holzmann, and D. M. Ceperley, Phys. Rev. B **101**, 165125 (2020).